

Short communication

Predicting tidal flooding of urbanized embayments: A modeling framework and data requirements

T.W. Gallien*, J.E. Schubert, B.F. Sanders

Department of Civil and Environmental Engineering, University of California, Irvine, UC Center for Hydrologic Modeling, United States

ARTICLE INFO

Article history:

Received 22 July 2010

Received in revised form 18 January 2011

Accepted 20 January 2011

Available online 26 February 2011

Keywords:

Coastal flooding
Inundation modeling
Overtopping
Flood mapping
Urban flooding
LiDAR

ABSTRACT

Numerous urbanized embayments in California are at risk of flooding during extreme high tides caused by a combination of astronomical, meteorologic and climatic factors (e.g., El Niño), and the risk will increase as sea levels rise and storminess intensifies. Across California, the potential exists for billions of dollars in losses by 2100 and predictive inundation models will be relied upon at the local level to plan adaptation strategies and forecast localized flood impacts to support emergency management. However, the predictive skill of urban inundation models for extreme tide events has not been critically examined particularly in relation to data quality and flood mapping methodologies. With a case study of Newport Beach, California, we show that tidal flooding can be resolved along streets and at individual parcels using a 2D hydraulic inundation model that captures embayment amplification of the tide, overtopping of flood defenses, and overland flow along streets and into parcels. Furthermore, hydraulic models outperform equilibrium flood mapping methodologies which ignore hydraulic connectivity and are strongly biased towards over-prediction of flood extent. However, infrastructure geometry data including flood barriers, street and parcel elevations are crucial to accurate flood prediction. A real time kinematic (RTK) survey instrument with an error of approximately 1 cm (RMSE) is found to be suitable for barrier height measurement, but an error of approximately 15 cm (RMSE) typical of aerial laser scanning or LiDAR is found to be inadequate. Finally, we note that the harbor waterfront in Newport Beach is lined by a patchwork of public and private parcels and flood barriers of varied designs and integrity. Careful attention to hydraulic connectivity (e.g., low points and gaps in barriers) is needed for successful flood prediction.

© 2011 Elsevier B.V. All rights reserved.

1. Introduction

Absolute sea levels are projected to rise 1–1.4 m along the California coast in the next century (Cayan et al., 2009). A statewide impact assessment indicates a wide range of critical infrastructure including 5600 km of roadways, 450 km of railways, 29 wastewater treatment facilities and countless buildings and contents valued at over \$100 billion dollars are at risk (Heberger et al., 2009), and there have been calls for statewide adaptation planning and action at the local level. A California Assembly Bill, introduced in the 2009–2010 legislative session, would require local entities to develop “sea level action plans” that estimate the financial costs of sea level rise and develop plans to prevent or mitigate damage to development, infrastructure and habitats. Local, regional and global planning efforts of a similar nature are underway in many parts of the world, particularly in the UK (Defra, 2005; Hall et al., 2005, 2006). A recent

investigation of coastal flooding and erosion scenarios demonstrates natural coastal erosion yields significant flood risk benefits and urges managed retreat as a necessary adaptation strategy (Dawson et al., 2009). Another study urges a dynamic approach to flood risk management and suggests managed retreat as a tool to facilitate estuary migration (Pethick, 2001). Broad actions to reduce future flood impacts are also encouraged: the reduction of greenhouse gas emissions, avoidance of anthropogenic subsidence enhancement, upgrading flood defense infrastructure and control of coastal floodplain development (Nicholls, 2002). Globally, four major impacts have been identified from sea level rise analyses: wetland and lowland inundation and displacement, shoreline erosion, enhanced storm flooding and increased salinity effecting estuaries and potentially, fresh water aquifers (Nicholls, 2002, 2007).

This study is focused on coastal flooding, and the manifestation of “sea level rise” as an increase in the frequency and severity of extreme events. From a California flooding perspective, the greatest threat is posed by the coincidence of high tides and winter storms that cause a surge in ocean height and excite wave activity. A strong winter storm can yield a surge of 0.2–0.3 m over a period of hours (Flick, 1998), in contrast to the Gulf and Atlantic Coasts where storm surges on the order of meters are possible and have been the focus of coastal

* Corresponding author. Tel.: +1 9498244327.

E-mail addresses: tgallien@uci.edu (T.W. Gallien), j.schubert@uci.edu (J.E. Schubert), bsanders@uci.edu (B.F. Sanders).

URL: <http://www.sanders.eng.uci.edu> (B.F. Sanders).

flooding studies (e.g. Bunya et al., 2010; Sheng et al., 2010). The El Niño Southern Oscillation (ENSO) is also important. During its warm phase, the jet stream intensifies, splits and redirects cyclonic systems across California and this can lead to 0.1–0.3 m higher water ocean levels over a period of days or weeks (Flick, 1986; Storlazzi & Griggs, 2000). Tides in California are a mixture of diurnal and semi-diurnal constituents and exhibit a fortnightly spring–neap cycle in the diurnal range with a spring range of 2–3 m (Flick, 1998; Zetler & Flick, 1985). Consequently, the risk of flooding is heightened under spring tide and El Niño conditions. Indeed, extensive flooding and damage has occurred during past El Niño winters with coincident spring tides and storms, while only minor flooding has resulted from spring tides in the absence of storm activity or from strong storms coincident with neap tides (Flick, 1998).

The preceding history highlights the sensitivity of California flood impacts to relatively small (10–30 cm) increases in ocean heights beyond astronomical high tide predictions, as well as the importance of wave-driven flooding. This also focuses attention on factors that, in a warmer climate, could further raise high water levels: higher mean sea levels, larger tidal amplitudes, and increased storminess characterized by greater winds and waves and lower atmospheric pressure (Bromirski et al., 2003; Flick et al., 2003; Graham & Diaz, 2001).

In California, development and infrastructure at risk of coastal flooding is concentrated around urbanized embayments that are sheltered to some extent from ocean swell and large wind waves that impact the open coast (Heberger et al., 2009). San Francisco Bay serves as one example in the northern part of the state, while Marina del Rey, the ports of Los Angeles and Long Beach, Huntington Harbor, Newport Harbor, and San Diego Bay provide examples further south. In sheltered embayments, portions of the bay front are guarded by sea walls and levees and a central issue for development and infrastructure impact assessment is the potential for overtopping and subsequent inundation. Overtopping flows may result in damaging high velocity currents and can be expected to flood low lying terrain first and progressively deepen as overtopping continues. The overtopping flow rate per unit width is scaled by the height difference between the ocean and the barrier, similar to a hydraulic weir. Hence, the flow rate can be expected to rise and fall with the rise and fall of the ocean tide and surge. A key issue becomes the total volume of water that overtops defenses, which corresponds to the integral of the overtopping flow rate per unit width over the length of sea walls and the duration of a flood event.

Concurrently, in the context of flood risk management, there has been a trend towards high-resolution social and economic impact assessment (parcel and street scale) that relies on high-resolution flood intensity data (flood depths and velocity) (Ermts et al., 2010). Aerial laser altimetry or LiDAR is capable of measuring ground elevation with a spatial resolution (~1 m postings) and vertical accuracy (~10–15 cm) that is adequate for many flood mapping applications (Colby & Dobson, 2010; Gesch, 2009; Gallegos et al., 2009; Sanders, 2007; Webster et al., 2004), and the National Research Council (NRC) has called for a National LiDAR terrain modeling effort for flood mapping purposes (National Research Council, 2009). However, multiple studies have noted that low relief areas are especially sensitive to terrain representation (Bates et al., 1997; Colby & Dobson, 2010). A Canadian study conducted at Charlottetown, Prince Edward Island utilized LiDAR to map flood risk and results indicated that LiDAR can provide high resolution data for digital elevation models and flood risk hazard mapping, however abrupt elevation changes such as wharves, sea walls and cliffs are inadequately resolved for inundation modeling (Webster et al., 2004). Néelz et al. (2006) investigated remotely sensed data for flood modeling applications and found significant LiDAR limitations for resolving walls, banks and other hydraulically significant features and emphasizes the need to conduct a high accuracy RTK survey of hydraulically important features. A study on Convey Island (UK) highlights the complexity and uncertainty inherent to urban flood modeling and urges uncertainties such as flood defense breaching, failure and localized flow sources and

sinks to be explicitly incorporated into model predictions (Brown et al., 2007). Cartesian or raster grid modeling of coastal flooding resulting from sea level rise emphasizes the importance of coastal topographic complexity and advocates enforcement of fine scale features such as ditches and dikes within the model (Poulter & Halpin, 2008). In a recent analysis of LiDAR elevation data for delineation of land vulnerable to sea level rise, Gesch (2009) suggests that future assessments will prove more useful and reliable if detailed and infrastructure information included. Additionally, Heberger et al. (2009) calls for the survey, assessment and cataloging of existing flood defenses along with more rigorous local modeling to guide coastal adaptation. Collectively, these studies illuminate the need to incorporate flood defense barriers and associated uncertainties to develop robust local inundation models, and not simply rely on LiDAR data alone. However, the level of accuracy required for the heights of barriers subject to overtopping is not clear, nor is the benefit of hydraulic flood routing methodologies over “bathtub” type models (e.g. Heberger et al., 2009; Knowles, 2009) that determine flood zones by a simple comparison of ocean and land heights.

The objective of this paper is to describe a framework for regional, high resolution mapping of tidal flooding impacts in urbanized embayments and to present a case study of Newport Beach, California that reveals the predictive skill of high-resolution inundation models including a characterization of prediction uncertainties related to data quality and modeling methodologies. This information is essential for meaningful sea level rise impact assessment and effective adaptation planning and emergency management. While wave-driven flooding is also important in California, particularly along the open coast, it is less important in sheltered embayments and is not addressed here in order to focus on tidal flooding.

2. Methods

2.1. Site description

Newport Beach is an economically important, densely populated California coastal community located approximately 70 km southeast of Los Angeles shown in Fig. 1. The City of Newport Beach encompasses one of the largest estuarine embayments in California, Newport Harbor, and is geographically divided into three zones; high relief elevations on the eastern portion of the city, elevated marine terraces on the northwestern portion of the city and urban coastal lowlands which include Balboa Peninsula and Balboa Island, the foci of the investigation. The Peninsula shelters Newport Harbor from swell and large wind waves from the Pacific Ocean, so the outer Peninsula shoreline is exposed to wave-driven flooding while the inner harbor is exposed to tidal flooding. Sand dunes correspond to the highest topography along the Peninsula and therefore constitute its flood defense, while the inner harbor is protected primarily by concrete flood walls. Balboa Island is one of the most densely populated communities in the United States and is fully encircled by a concrete flood wall. Both Balboa Island and Peninsula have experienced several episodes of flooding in the past century including Hurricane Liza generated swell in September 1968 which impacted the outer Peninsula and El Niño Southern Oscillation storm events in 1972–1973, 1982–1983, 1987–1988 and 1997–1998. More recently, on January 10, 2005 the combination of an extreme high tide and a cyclonic low pressure storm system caused tidal flooding of both Balboa Peninsula and Balboa Island. As described in Section 2.3, the January 10 event was thoroughly documented by the City of Newport Beach personnel and therefore serves as a validation dataset for this study.

2.2. Topographic and bathymetric data

The City of Newport Beach provided LiDAR data and orthoimagery from a 2006 city commissioned survey. Original orthoimagery was

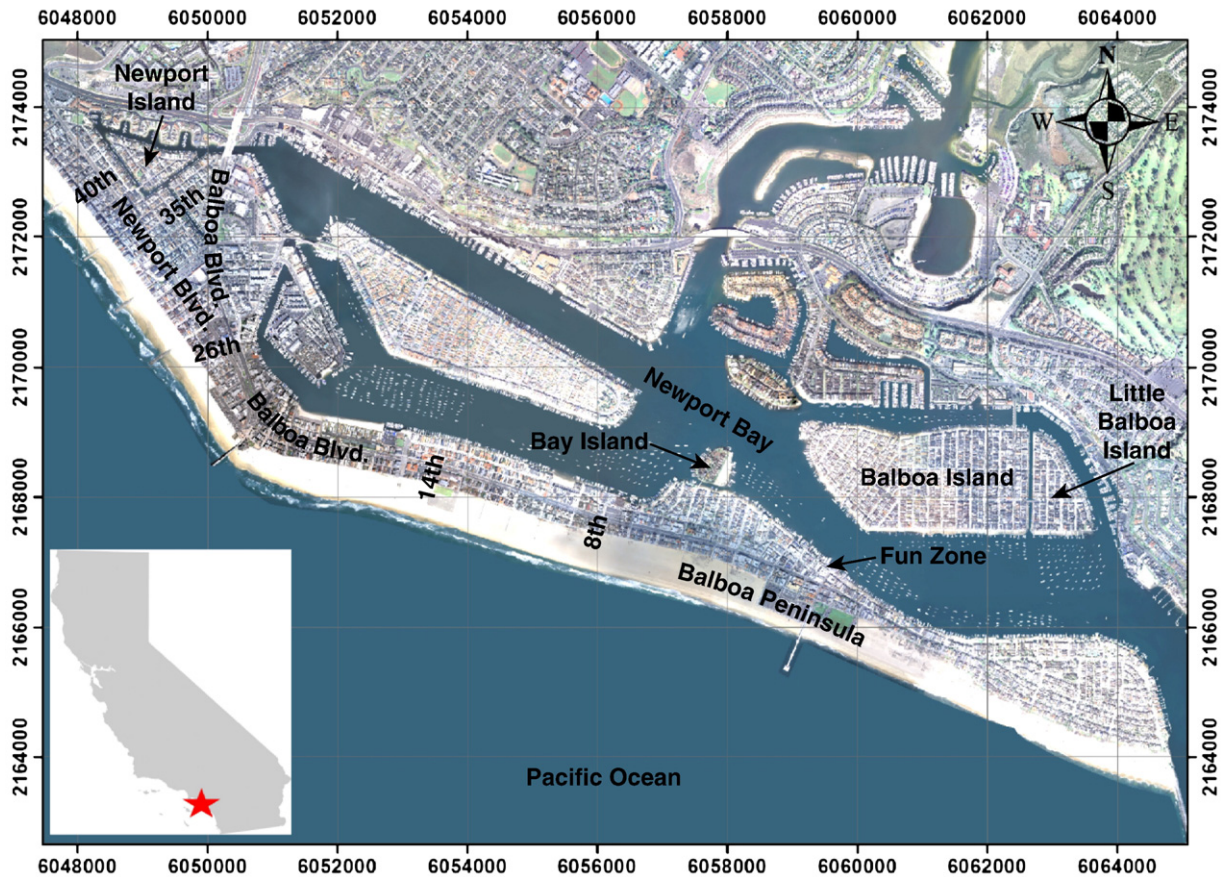


Fig. 1. Newport Beach, California site.

provided at 7.62 cm horizontal resolution but decreased to 30 cm to facilitate data management. The LiDAR survey covered 146 km² divided into 262 tiles and over 53.5 million surface samples (point cloud data). All coordinates were referenced to the NAD 1983 California State Plane Zone VI (feet) coordinate system and the NAVD 1988 (NAVD feet) vertical datum. All modeling was performed in US units and output converted to SI units. Of the 262 tiles, only 112 represented the coastal area of interest, the balance of the tiles was discarded. The final LiDAR dataset contained approximately 10 million irregularly spaced points with a vertical accuracy of 0.182 m (RMSE) yielding a linear accuracy of 0.357 m (Maune et al., 2007). Upper and Lower Bay bathymetry in NAVD was obtained from two U.S. Army Corps of Engineers, Los Angeles District commissioned surveys in 2003 and 2005 and represent 1 m and 3 m resolutions, respectively. Three arc-second resolution offshore bathymetry from the National Geophysical Data Center (NGDC) was retrieved from the Southern California Coastal Ocean Observing System (SCCOOS) website. Offshore bathymetry resolution was approximately 100 m and height was specified relative to mean lower low water (MLLW) which differs from NAVD by 5.49 cm at Newport Beach. Given that offshore bathymetry data corresponds to depths greater than 10 m, the relative datum error ($\Delta z/h$, normalized by depth) is less than 1% and inconsequential for flooding analyses. That is, testing revealed a 5.49 cm offshore bathymetry difference negligibly affected maximum water levels (*ca.* 0.05 cm) and consequently did not affect flood extent, therefore no height corrections were made. From the datasets, shown in Fig. 2, over 12 million points that spanned the entirety of Newport Bay topography and bathymetry were merged into a single pointfile with a NAD83 and NAVD datums, and inverse distance weighted interpolation was used to create a 3 m digital terrain model (DTM) in a raster (Cartesian grid) format.

LiDAR survey returns from the tops of flood barriers such as sea walls were minimal; therefore accessible barriers were surveyed using a Magellan ProMark 3 Real Time Kinematic (RTK) survey rover unit (Magellan, Santa Clara, CA) and Orange County Real Time Network base station (FVPK) corrections (Orange County Public Works, 2009). The Magellan unit is capable of centimetric vertical accuracy in fixed mode. A Magellan RTK trial application similar to the Newport Beach study using a 10 km baseline achieved a vertical root mean square error (RMSE) of 16 mm (Magellan, 2007). Pre-survey testing at a local geodetic control point in fixed mode yielded an RMSE of 9.87 mm whereas an in situ benchmark accuracy test revealed a 13.5 mm RMSE. The ProMark 3 was operated in fixed mode with site baselines ranging from 4.59 km to 8.61 km.

2.3. Flood event description

During the January 10, 2005 flood event, the City of Newport Beach employees were dispatched to manage and photodocument inundation which consisted of multiple flood zones on the Peninsula and Balboa Island. This resulted in 85 digital photographs that, in combination with eyewitness accounts from the City of Newport Beach employees obtained through two interview sessions and email communications, provided essential data for model validation and uncertainty analysis. Eighteen digital photographs of Balboa Island flooding and 67 of Peninsula flooding were manually examined for location, perspective and wet/dry interfaces near identifiable features to determine water surface elevation. Flood extent was then manually mapped in ArcGIS (ESRI, Redlands, CA) by extrapolating the water height to all hydraulically connected terrain at or below this elevation, based on the raw LiDAR point cloud data and using the georeferenced

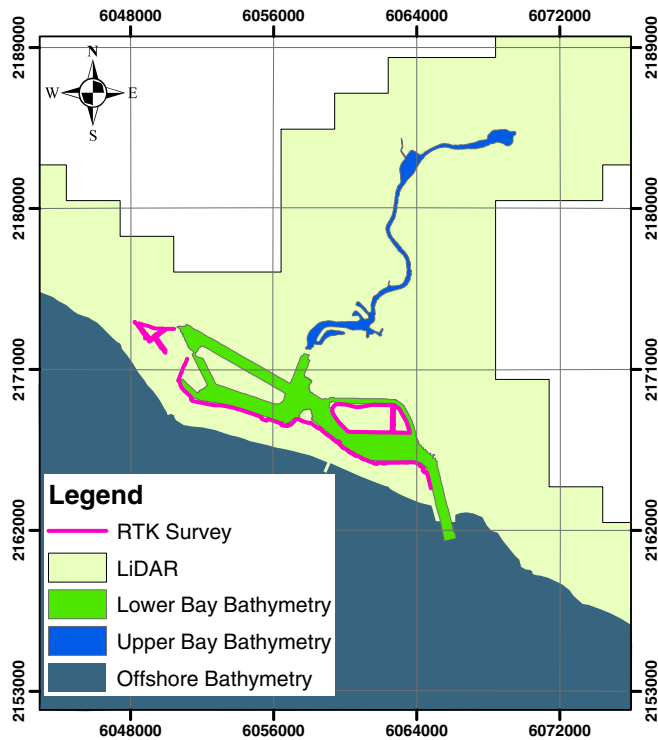


Fig. 2. Data sources.

orthoimagery as a guide. Eyewitness accounts were used in a similar manner to delineate flood zones southwest of Newport Island and south of Bay Island. In this case, site-specific reports of flood depths served as the starting point for the manual extrapolation procedure. Flood extent data was saved as a GIS polygon layer.

The January 10, 2005 flood event generated an observed tide height of 2.356 m (NAVD) at Los Angeles (NOAA Buoy 9410660), the nearest monitoring station located 38 km northwest of the study site. The observed tide was 0.218 m above the NOAA predicted tide, highlighting the sensitivity of flood impacts to small increases in the ocean height. The total ocean height in Newport Bay was not measured but may be inferred through the City of Newport Beach photodocumentation which depicts water minimally overtopping a sea wall section at the Northwest corner of Balboa Island. RTK survey data indicates a wall height here of 2.357 ± 0.057 m (NAVD), which compares well with the Los Angeles observation, but the interior harbor water level may have actually been higher than the observed Los Angeles tide because: (a) overtopping of the wall was observed and (b) tidal amplification across the length of the harbor has been observed in preliminary modeling.

To approximate the time-dependent change in ocean height $\eta(t)$ at Newport Harbor over a 12 hour period on January 10, 2005, for use in hydraulic modeling described later, oscillatory and solitary wave equation solutions were summed as follows,

$$\eta(t) = H_0 + a \cos \frac{2\pi(t-t_1)}{t_2} + b \operatorname{sech}^2 \left(\frac{t-t_3}{t_4} \right) \quad (1)$$

where t represents time, H_0 is the still water height, a is the oscillatory wave amplitude, b is the solitary wave amplitude, t_1 is the oscillatory wave phase, t_2 is the oscillatory wave period, t_3 is the solitary wave phase, and t_4 is the solitary wave duration parameter. Two water height parameterizations were used to account for uncertainty in the ocean height, as shown in Table 1. The first (Tide 1) assumes that a height of 2.356 m (NAVD) was attained inside the harbor at the mid-

bay point where overtopping was observed. The second (Tide 2) assumes that a height of 2.356 m (NAVD) was enforced at the offshore boundary and therefore corresponds to a higher mid-bay water elevation. Tide 1 parameters were obtained by an iterative forward modeling technique using the hydraulic model described in Section 2.6, i.e., a and b were changed until the inner harbor tide achieved the desired height. The mid-bay height reported in Table 1 for Tide 2 was computed from a single forward application of the model. Both tides were monitored at the inlet of the bay and were identical to the boundary condition tide heights. These results show that tides are amplified within the bay by approximately 5 cm, or 6% of the total displacement from the still water height specified offshore. The amplification differs modestly across the lower bay. In the central open water area of the bay the amplification is 4.9 cm, and at the far western end of the bay, the amplification is 7.0 cm.

2.4. Modeling framework

An effective framework for modeling inundation of coastal embayments has emerged from the literature (Bates et al., 2005; Brown et al., 2007; Purvis et al., 2008; Dawson et al., 2009; Knowles, 2009). This involves simulation models that depict specific events, as well as sampling strategies such as Monte Carlo methods that make use of many event simulations to characterize inundation probabilities and associated uncertainties. Here we are focused on the accuracy and uncertainty of individual event simulations, in relation to the data sources and modeling methodologies used. Event simulation at the local scale (<100 km) has been approached by establishing a local simulation domain wherein hydraulic models are applied to simulate spatial and temporal changes in embayment water heights in response to boundary forcing. For example, Knowles (2009) established a San Francisco Bay model domain that was externally forced seaward of the Golden Gate Bridge by a time series which accounts for the total ocean height, a combination of tidal and non-tidal (e.g. storm surge and atmospheric pressure changes) factors, as well as inland streamflow. Similarly, Purvis et al. (2008) present a domain along the southern shoreline of the Bristol Channel of Great Britain that is externally forced by a spatially variable ocean height to account for longitudinal changes in the channel tide. Collectively, studies such as these have shown that a nesting approach can be used whereby large scale models or observational data are used for boundary forcing of a local simulation model, which is then relied upon to account for local details such as tidal amplification and/or dissipation within the embayment, flooding and drainage with the rise and fall of the local embayment water surface, and the effect of control structures such as levees, sea walls, storm sewers, temporary sand berms, and sand bags.

Within this general modeling framework, inundation mapping has been handled in two distinct ways. One approach has been to constrain the hydraulic model domain to regularly submerged terrain, and to extrapolate flood extent by comparing terrain heights to the nearest available embayment height (e.g. Knowles, 2009). Those areas that fall below the embayment height are assumed to flood, so the assumption is that hydraulic flow paths exist and the flood is sustained sufficiently long to fill the impacted region up to the height of the embayment. We term this an equilibrium flood mapping

Table 1
Total water height parameterizations. All heights in meters relative to NAVD.

Name	Offshore height (m)	Mid-bay height (m)	H_0 (m)	a (m)	b (m)	t_1 (h)	t_2 (h)	t_3 (h)	t_4 (h)
Tide 1	2.311	2.356	1.408	0.690	0.213	12	-3.8	8.2	2.3
Tide 2	2.356	2.411	1.433	0.704	0.219	12	-3.8	8.2	2.3

method. Variants of this approach can be devised to account for protection by levees and sea walls, but the assumption is that inundation occurs instantaneously upon exceeding the overtopping threshold. The alternative method is to extend the hydraulic model domain to all areas subject to episodic inundation and to make flood mapping an integral part of the hydraulic model analyses (e.g. Purvis et al., 2008). Failures of protective barriers such as levees can be integrated into both methods (e.g. Brown et al., 2007), but only the latter approach accounts for storage and resistance effects and provides detailed information about the velocity and depth distribution which is necessary for impact assessment (e.g. Ernts et al., 2010).

Two-dimensional Godunov-type finite volume models based on shallow-water wave theory are relatively new to flood inundation modeling but have been shown to support an accurate and stable prediction of inundation dynamics (flooding and drainage) in complex urban landscapes (e.g. Gallegos et al., 2009). These models have overcome long standing stability and conservation problems posed by a moving wet/dry interface which constitutes a singularity in the governing equations (e.g. Begnudelli & Sanders, 2006), and allow for a wide range of flow regimes to be resolved including supercritical breach flows without case-specific parameter tuning. Godunov-type shallow-water models therefore constitute an attractive basis for integrated embayment flood event modeling as described above, i.e., seamlessly resolving embayment long wave dynamics, overtopping, breach flows, and overland flow into low lying terrain. To maintain computational efficiency, representation of terrain topography within the flood model requires simplification, particularly in areas unaffected by flooding or where the flood threshold elevation to water level comparison is inconsequential (e.g. high elevation or offshore areas). These topological simplifications, known as “coarsening” in the geomatics field, must be performed carefully to retain correct hydraulic connectivity for flood propagation accuracy. Fewtrell et al. (2008) examined the effects of digital terrain coarsening and suggests that model resolution should correspond to hydraulic flow path length scale. Purvis et al. (2008) coarsened a high-resolution raster DTM to support application of a Cartesian grid model, and raster cells containing flood barriers were assigned the height of the barrier. Alternatively, in an unstructured grid model, Schubert et al. (2008) used polylines and polygons delineating flood barriers to constrain the computational mesh for correct hydraulic connectivity.

Several types of data are critical to the success of this modeling framework. Elevation data for all features that constrain or affect the flow of water (bare earth heights, sea wall heights, etc.) are essential (e.g. Gallegos et al., 2009; Webster et al., 2004; Wilson & Atkinson, 2005), and land surface data can be important for characterizing vegetative and non-vegetative flow resistance (e.g. Mason et al., 2007; Schubert et al., 2008). Time series of the total ocean height at boundaries is important as well for model forcing purposes, and in some cases additional time-series data including stream flow entering model boundaries, precipitation data, and wind data may be required. As was mentioned in the introduction, the aim here is to critically examine the uncertainty of flood maps based on uncertainty in topographic data, barrier height data in particular, uncertainty in boundary forcing data, and the use of dynamic versus equilibrium flooding mapping methods.

2.5. Equilibrium flood mapping

Equilibrium flood mapping, or the “bathtub” approach, is based on a comparison of the maximum total water height and ground elevation; land lower than the maximum total water height is assumed to flood. Hydraulic connectivity may or may not be considered, and the latter option is straightforward to implement in GIS which has made it popular for large scale sea level rise impact assessment (e.g. Poulter & Halpin, 2008). Equilibrium flood mapping methods therefore rely exclusively upon DTM quality and resolution

and do not consider hydraulic factors such as connectivity, storage and resistance. Consequently, flooding thresholds such as wharves, embankments and flood defense walls do not constrain the flood extent even if they are incorporated into the DTM.

2.6. Hydraulic flood mapping

Godunov-type finite volume codes have previously been used for coastal embayment modeling (Arega & Sanders, 2004; Cea et al., 2006; Sanders, 2008) as well as urban flood inundation modeling (Villaneueva & Wright, 2006; Schubert et al., 2008; Sanders et al., 2008; Gallegos et al., 2009) and therefore represent a good candidate for integrated hydraulic modeling of coastal flooding events. Godunov-type schemes rely on an approximate Riemann solver to compute mass and momentum fluxes along the edges separating neighboring computational cells (Guinot, 2003; Toro, 2001). This approach accommodates highly variable terrain found in urban environments such as abrupt elevation changes, flood defenses and streets and, without any case specific parameter tuning resolves highly transient transcritical flows that may result from overtopping and/or failure of flood barriers. Here, the unstructured grid model BreZo is used (Begnudelli et al., 2008; Sanders, 2008). An unstructured grid enables computational resources to be focused on lowlands subject to flooding and drainage. In particular, Gallegos et al. (2009) recommend that streets be resolved by approximately three computational cells for accuracy purposes. BreZo benefits from numerous modeling studies aimed at the robust handling of wetting and drying over irregular topography (Begnudelli & Sanders, 2006; Bradford & Sanders, 2002), studies to minimize numerical dissipation so physically meaningful resistance parameters can be used (Bradford & Sanders, 2005; Begnudelli et al., 2008), and efforts to improve computational efficiency (Begnudelli et al., 2008; Sanders, 2008). For example, BreZo uses a local time stepping (LTS) scheme that assigns cells a time step of either Δt , $2\Delta t$, $4\Delta t$, the largest time step that satisfies the local Courant, Friedrichs, Lewy (CFL) condition. This prevents small cells in the domain from dictating a small time step in all cells, and can reduce run times by over 50% compared to a commonly used global time stepping schemes (Sanders, 2008). Flux calculations and solution updates are carefully sequenced to maintain time-wise accuracy and to conserve mass and momentum.

The unstructured grid or mesh used by BreZo stores a combination of vertex and cell-based data along with initial and boundary conditions. Ground elevation (or barrier height) is assigned at vertices, while resistance parameters are assigned to cells. The version of BreZo used here is formally first order accurate. However, use of vertex-based terrain data supports second order convergence rates in natural topography flood simulation where terrain truncation error limits accuracy (Begnudelli et al., 2008).

The computational mesh used by BreZo corresponds to a constrained Delaunay triangulation of the simulation domain. The domain is bounded by the DTM extent and therefore encompasses all above and below-water terrain in the vicinity of Newport Bay, and extends several kilometers offshore. The mesh was generated using Triangle (Shewchuk, 1996) which allows maximum cell area, minimum vertex angle, and edge position constraints. Constraints were used in several ways to promote accuracy and computational efficiency. A minimum angle constraint of 30° was used to avoid stability problems that arise from highly acute angles, spatially variable area constraints were used to focus computational resources on the urbanized lowlands subject to flooding and to gradually coarsen the grid with increasing ocean depth, and edge constraints were used so mesh vertices (and edges) are aligned with land surface features subject to overtopping, sea walls and embankments in particular, for accurate depiction of overtopping heights. That is, by aligning mesh vertices with local maxima in the topography, vertex heights are accurately interpolated from the DTM. Edge location data was obtained by developing a polyline of all flood barriers (sea walls

and embankments) from RTK survey data and orthoimagery of the site. Unique node and edge identifiers were associated with mesh vertices aligned with flood barriers so that vertex heights could easily and accurately be estimated from RTK survey data, as an alternative to the DTM. In several places, fine-scale curvature in flood barriers forced localized mesh refinements far beyond the desired resolution similar to the meshing challenges reported by Tsubaki and Fujita (2010), so a manual smoothing procedure was used which effectively pushed the flood wall offshore a short distance to eliminate unnecessary refinement and improve computational efficiency. The previously mentioned identifiers then facilitated the assignment of heights based on nearby, but not perfectly aligned, flood barrier data.

The mesh resulting from this process consisted of approximately 500,000 cells. The finest mesh resolution (ca. 3.5 m) corresponds to Balboa Peninsula and Balboa Island to adequately resolve street depressions which channel spreading flood water (Gallegos et al., 2009). An intermediate resolution was used for harbor channels and open water areas of the bay (ca. 25 m), and the coarsest resolution (ca. 300 m) was used offshore and at high elevations. Additional intermediate resolutions were used for smooth transitions between these zones.

Vertex elevations were assigned in four different ways to examine uncertainties related to topographic data uncertainty, giving rise to what we term Meshes 1–4, while the meshes share a common horizontal distribution of vertices. Mesh 1 corresponds to vertex heights interpolated directly from the DTM using inverse distance weighted interpolation. Mesh 2 corresponds to Mesh 1 for all points except those flagged as flood barriers, where heights were instead linearly interpolated from RTK survey data. Hence, flood map uncertainty associated with narrow flood barriers that are not captured by the LiDAR data will be revealed by comparing results from Meshes 1 and 2. Mesh 3 was introduced to examine the uncertainty in flood maps associated with uncertainty in RTK recorded heights (i.e., limited vertical accuracy). A random vertical offset was added to each RTK survey point and then mesh vertex heights were interpolated again as with Mesh 2. The random offset is characterized by a mean of zero and a standard deviation calculated for that point based on its 95% confidence level (reported by the RTK unit). Mesh 4 was constructed identically to Mesh 3, except that the random offset was based on the LiDAR RMSE which is roughly an order of magnitude larger than the RTK height uncertainty. The Newport Beach LiDAR survey yielded insufficient wall returns to estimate sea wall elevations, but if the flood walls had been wider as is typical of an earthen levee, then there would have been an adequate number of returns. Hence, Mesh 4 provides insight into flood map uncertainty resulting from the vertical accuracy typical of commercial LiDAR data. Table 2 summarizes the attributes of each mesh.

2.7. Modeling scenarios

A matrix of ten modeling scenarios were considered to examine all of the previously discussed effects (e.g., uncertain ocean heights, wall heights, and flood mapping), as shown in Table 3. Scenarios 1–4 use Mesh 1 which consider only DTM derived elevations and explore the effects of ocean height and flood mapping methodology. Scenarios 5 and 6 utilize Mesh 2, depicting the flood walls, and explore the effects

Table 2
Computational meshes developed for analysis of flood mapping accuracy and uncertainty.

Mesh	DTM data	RTK data	Wall height resampling	Resampling basis
1	Yes	No	No	–
2	Yes	Yes	No	–
3	Yes	Yes	Yes	RTK error
4	Yes	Yes	Yes	LiDAR error

Table 3
Modeling scenarios.

Model scenario	Mesh number	Tide parameters	Embayment amplification	Flood mapping
1	1	2	No	Equilibrium
2	1	2	Yes	Equilibrium
3	1	1	Yes	Hydraulic
4	1	2	Yes	Hydraulic
5	2	1	Yes	Hydraulic
6	2	2	Yes	Hydraulic
7	3	1	Yes	Hydraulic
8	3	2	Yes	Hydraulic
9	4	1	Yes	Hydraulic
10	4	2	Yes	Hydraulic

of ocean height and topographic uncertainties. Scenarios 7 and 8 utilize Mesh 3 and, when compared to Scenarios 5 and 6 reveal the importance of RTK measurement uncertainty. Lastly, Scenarios 9 and 10 utilize Mesh 4 and reveal the significance of limited vertical accuracy typical of LiDAR, when relied upon for depicting the threshold of overtopping.

Note that the tide referenced in Table 3 refers to the boundary forcing of the hydraulic model, except for Scenario 1 which ignores tidal amplification. In this case, the equilibrium flood mapping method is applied using the maximum height of the tide (2.356 m). Also, note that for Scenario 2, the hydraulic model was utilized to calculate tidal amplification and the bay was divided into several subdomains corresponding to the maximum calculated water level as shown in Fig. 3, the equilibrium flood mapping method was then applied using these tidally amplified water levels. Knowles (2009) used a similar approach when mapping flood zones around San Francisco Bay.

2.8. Fit measures

Several fit measures were used to quantify accuracies and uncertainties in flood extent predictions. An agreement fit measure, F_A , represents the intersection of predicted and observed flood extents divided by the union of the predicted and observed flood extent as follows,

$$F_A = \frac{E_p \cap E_o}{E_p \cup E_o} \quad (2)$$

where E_o and E_p represent the observed and predicted flood extent, respectively. A fit measure of zero and unity corresponds to no agreement and complete agreement, respectively. Secondly, an underprediction fit measure F_{UP} characterizes the fraction of flooded area observed, but not predicted as follows,

$$F_{UP} = \frac{E_o - E_p \cap E_o}{E_p \cup E_o} \quad (3)$$

and in this case a fit measure of zero and unity corresponds to no underprediction and complete underprediction, respectively. Lastly, an overprediction fit measure F_{OP} characterizes the fraction of flooded area predicted but not observed as follows,

$$F_{OP} = \frac{E_p - E_p \cap E_o}{E_p \cup E_o} \quad (4)$$

and in this case a fit measure of zero and unity corresponds to no overprediction and complete overprediction, respectively.

3. Results

Flood mapping of all scenarios was completed using a personal computer with an Intel 2.4 GHz dual core processor. Hydraulic flood

modeling proceeded with a 12 h simulation period over which the ocean tide was assumed to fall, rise and fall again according to Eq. 1. A time step of 0.05 s was used, and approximately 15 h of wall-clock time expired while BreZo executed each scenario. Maximum flood depths in each computational cell were computed internally by BreZo, saved to an output file at the end of the simulation, and then processed in ArcGIS to create flood maps for error analysis. Table 4 provides a summary of flood extent and fit measures from each of the scenarios considered.

3.1. Equilibrium flood mapping

Scenario 1 and 2 flood extent predictions, shown in Fig. 4a and b, indicate that the equilibrium mapping methodology significantly overestimates flood extent, both scenarios overpredicting $F_{OP} \approx 0.91$. Additionally, this overprediction is reflected in Scenario 1 by an agreement fit measure $F_A = 0.0880$ and an underprediction fit measure of $F_{UP} = 0.0003$. Considering that the equilibrium method considers neither hydraulic connectivity or flow barriers, these results of significant overprediction, minor or no underprediction and poor correct prediction are expected. For example, Little Balboa Island is defended by a minimally 2.529 m (NAVD) flood wall which is 17 cm above the assumed bay level, while Balboa Island is defended by a minimum 2.341 m (NAVD) flood wall. Along Balboa Peninsula, Scenario 1 shows that the main traffic thoroughfares would incur substantial inundation when in fact this area is defended by a combination of flood walls and embankments.

Scenario 2, which employs the spatially variable tidally amplified water height, shows an approximately 9% larger flood extent when compared to the Scenario 1 and yields a fit measure of $F_A = 0.0808$ and no underprediction, $F_{UP} = 0$.

3.2. Hydraulic flood mapping

3.2.1. Mesh 1: DTM-based topography

Scenarios 3 and 4 correspond to hydraulic flood mapping with Mesh 1 and Tides 1 and 2, respectively and are shown in Fig. 5a and b. Recall that in these scenarios, the hydraulic connectivity of the land surface is considered but only to the extent that it is captured by the LiDAR survey. Scenario 3 yields a flooded area of 0.968 km² and a fit agreement $F_A = 0.0967$. Like the equilibrium method presented

Table 4
Simulation results.

Scenario	Flood extent (km ²)	F_A	F_{OP}	F_{UP}	Comment
1	1.168	0.0880	0.9117	0.0003	Equilibrium
2	1.277	0.0808	0.9192	0	Flood maps
3	0.968	0.0967	0.9026	0.0007	Hydraulic maps
4	1.165	0.0883	0.9114	0.0003	w/o RTK
5	0.124	0.2256	0.4430	0.3314	Hydraulic maps
6	0.311	0.2148	0.6973	0.0879	w/ RTK
7	0.124	0.2189	0.4459	0.3352	Resampled
8	0.304	0.2164	0.6939	0.0897	w/ RTK error
9	0.566	0.1184	0.8275	0.0541	Resampled
10	0.760	0.1181	0.8663	0.0156	w/ LiDAR error

earlier, this represents a significant overprediction of flood extent. There are, however, significant differences between the hydraulic and equilibrium flood mappings results. For example, Scenarios 3 and 4 do not show flooding of the southeastern tip of the peninsula as do Scenarios 1 and 2. This is attributed to the existence of broad flood barriers that are adequately sampled by LiDAR and incorporated into the DTM.

Scenario 4, which uses a slightly higher ocean height, yields a larger flood extent and smaller F_A compared to Scenario 3, as shown in Table 4. Hence, a higher ocean height makes the agreement with the observed flooding worse. Results from Scenarios 3 and 4 also reveal a modest sensitivity of flood extent to ocean height. The difference between Tide 1 and 2 heights is 2.3% when normalized by NAVD elevation, and this corresponds to a 20% increase in flood extent.

3.2.2. Mesh 2: DTM- and RTK-based topography

Scenarios 5 and 6 correspond to hydraulic flood mapping with Mesh 2 and Tides 1 and 2, respectively and are shown in Fig. 5c and d. Recall that these simulations incorporate the RTK survey data which maps out narrow flood barriers. The result is a significant improvement in flood prediction accuracy compared to Scenarios 3 and 4. For example, $F_A = 0.2256$ and 0.2148 for Scenarios 5 and 6, which is approximately double the F_A values from Scenarios 3 and 4. These results highlight the importance of modeling narrow flood barriers. For example, narrow barriers preclude flooding on Little Balboa Island,

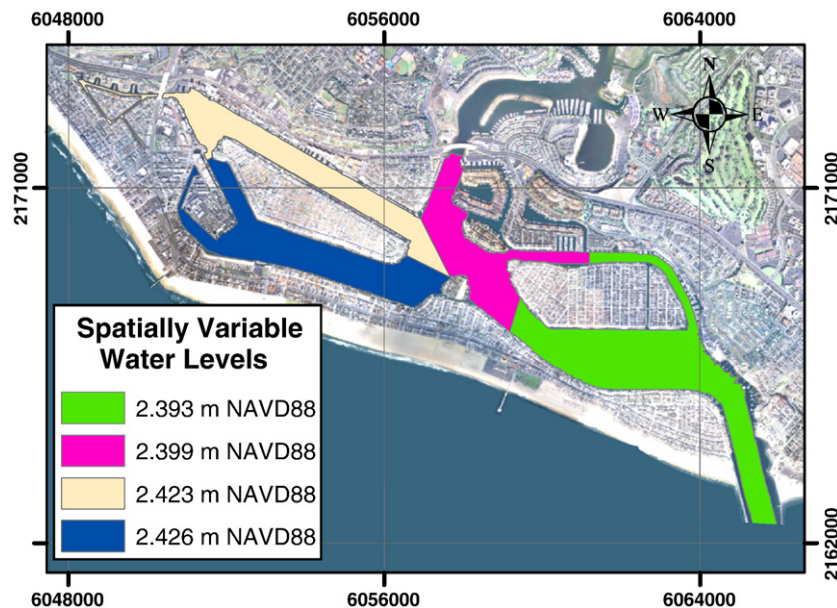


Fig. 3. Spatially variable maximum water level subdomains.

isolate Big Balboa Island flooding to the western portion of the island, and permit only localized flooding around Newport Island, the intersection Balboa and Newport Boulevards, the area South of Bay Island, and the wharf area known as the Fun Zone.

Table 4 also shows that Scenarios 5 and 6 underpredict flood extent more than Scenarios 3 and 4. A region of under-prediction is observed at 14th and Balboa Boulevard and several smaller regions of underprediction appear near the Newport Island and west of the Fun Zone. This implies that there are gaps in the flood defenses that have not been accounted for in the model. These could include low points in the sea wall that could not be accessed for the RTK survey, cracks in seawalls, seepage under sea walls, and/or back-flooding through drainage infrastructure.

With narrow flood walls included in the model, flood extent becomes far more sensitive to flood height. For example, flood extent is 150% larger for Tide 2 compared to Tide 1, which differ in height by only 2.3%. This is explained by the close proximity of the ocean height to thresholds of overtopping. Small increases in ocean height cause water to spill over a barrier and thus rapidly expand the flood zone.

3.2.3. Meshes 3 and 4: re-sampled topography

Scenarios 7 and 8 correspond to hydraulic flood mapping with Mesh 3, which utilizes re-sampled RTK-based topography based on RTK uncertainty and are shown in Fig. 5e and f. These results differ very little from Scenarios 5 and 6, respectively, as evidenced in Table 4. For example, flood extent increases by at most 2% (comparing Scenarios 6 and 8). This indicates that RTK accuracy is sufficient for flood mapping purposes.

Scenarios 9 and 10, shown in Fig. 5g and h, correspond to hydraulic flood mapping with Mesh 4, which utilizes re-sampled RTK-based topography based on LiDAR uncertainty. These results differ substantially from Scenarios 5 and 6, respectively, and are generally less accurate. For example, Scenarios 9 and 10 show significant overprediction on Balboa Island and Little Balboa Island, but flooding of the Fun Zone is significantly reduced and Bay Island inundation is absent. Extensive flooding on Balboa Boulevard between 26th and 8th is now shown, a large area of overprediction arises west of 8th street beach and widespread inundation is evident southwest of Newport Channel. Overall, the predominant effect of less accurate wall height (more uncertainty) is a significant increase in predicted flood extents corresponding to greater over-prediction. These results indicate that aerial LiDAR survey data are inadequate for capturing the threshold of overtopping from extreme high tides that may rise only centimeters above sea walls.

4. Discussion

Similar to many regions of the world, sea levels in California are projected to rise between 1 and 1.4 m in the next century (Cayan et al.,

2009) and over this time, adaptation of coastal developments, infrastructure, and natural resources such as wetlands is needed to avoid an increase in the frequency and severity of damaging flood events. Local flood impact assessments promise to identify the areas vulnerable to flooding, to measure and compare the benefits of proposed adaptation strategies such as higher sea walls, zoning changes, building policy changes, enhanced drainage infrastructure, beach nourishment programs, and even barriers similar to the Thames Barrier in London, England and the MOSE system near Venice, Italy. Local flood models may also prove valuable for emergency management, guiding evacuation efforts when necessary, supporting operational flood control efforts such as seasonal sand bagging, and supporting regional transportation systems with input about the viability of road and railways. The results of this study, however, suggest that flood extent prediction at or near the threshold of overtopping is extremely challenging and therefore subject to a high degree of uncertainty.

Four issues have been identified for effective studies: models must account for the full inventory of flood defenses, resolution and vertical accuracy must be focused in areas where elevation error and flood depth are similar orders of magnitude (e.g. uncertainty in overtopping thresholds must be considered, whereas offshore bathymetry effects are small), the uncertainty in the total ocean height must be considered, and detailed site specific information about hydraulic connectivity is important. The last of these points is magnified by the length of shoreline in coastal embayments, one of the principle lessons learned from Katrina where the extensive canal network created more opportunity for levee failure (U.S. Army Corps of Engineers (USACE), 2006).

Further improvement in flood map accuracy, beyond the level achieved here, will require careful scrutiny of privately owned property that may (or not) act to control flooding. Low points, cracks and gaps in sea walls are not uncommon and allow flooding that would not be predicted using the modeling methodology introduced here. For example, underprediction near 40th Street can be attributed to a low sea wall on a private property, based on photodocumentation collected by the City of Newport Beach which shows approximately 0.3 m of water over the back patio area and flowing onto the street. As another example, underprediction of flood extent near the intersection of 35th and Balboa Boulevard can be attributed to underground storm drainage communication. Through a calibration process, observations such as these could be used to further improve the accuracy of the model.

A validated regional hydraulic inundation model that is responsive to oceanographic, meteorologic and terrestrial forcing is the appropriate starting point when planning for the impacts of climate change, such as higher sea levels, higher tides and increased storminess. However, observations of flood extent and embayment levels across

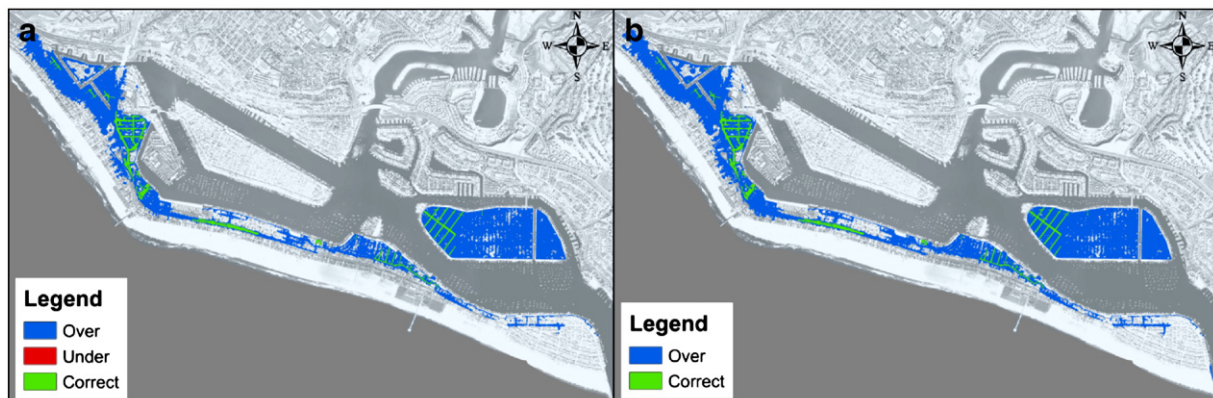


Fig. 4. Equilibrium flood mapping results for Scenario 1 (a) and Scenario 2 (b).

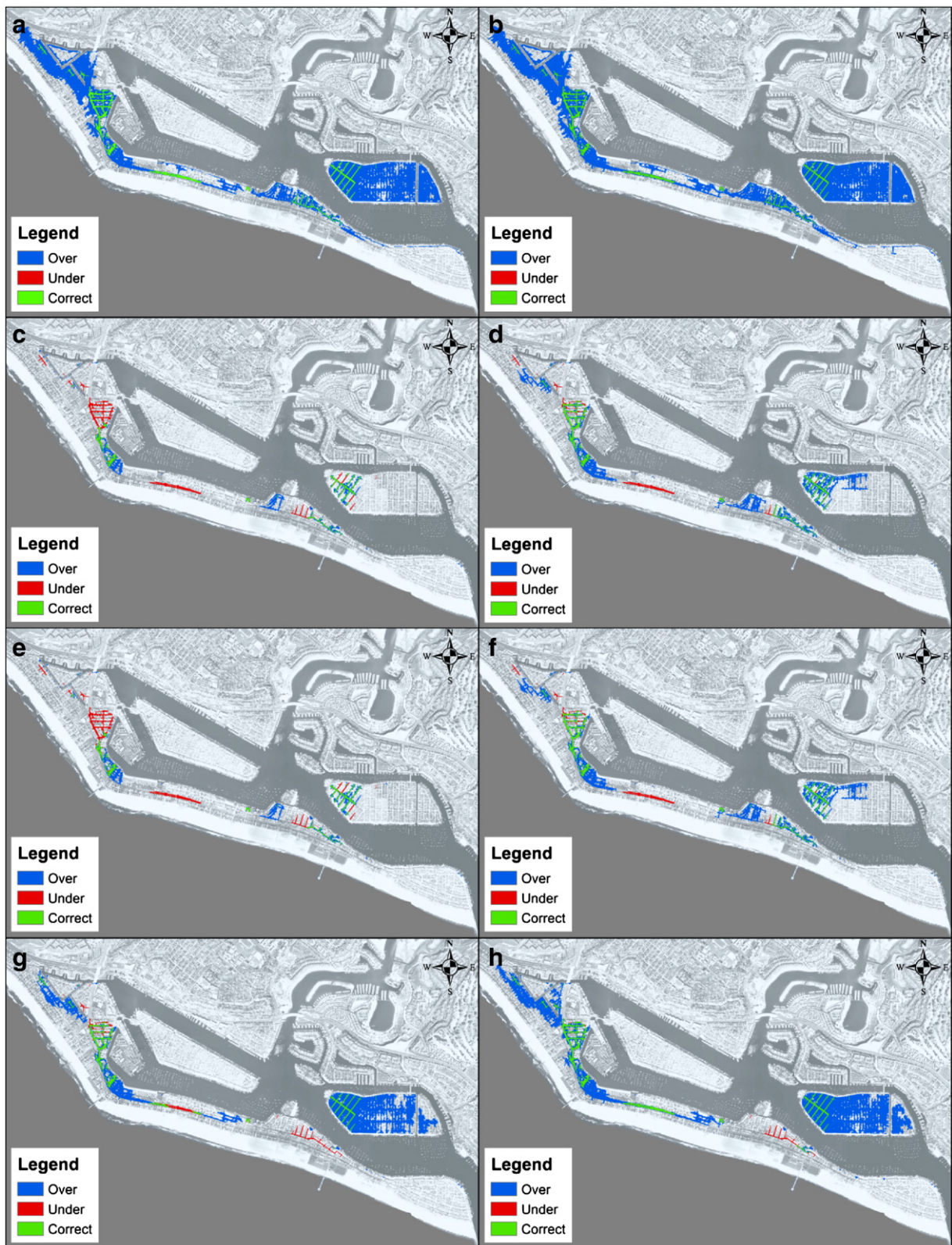


Fig. 5. Hydraulic flood mapping results for Scenario 3 (a), Scenario 4 (b), Scenario 5 (c), Scenario 6 (d), Scenario 7 (e), Scenario 8 (f), Scenario 9 (g) and Scenario 10 (h).

California are presently scarce which stands to hamper calibration and validation efforts. Available validation sets are limited to photographic reconstruction and are subject to manually referenced errors in water level which can cause a significant change in observed water level, for instance a water level elevation error of order 2–3 cm may vary in observed flood area 3–25% depending on location and hydraulic

connectivity. These issues emphasize the need for a coordinated monitoring program, which should include embayment tide levels and surveyed observations of flood zones (e.g., extents and depths). Experience from this study suggests that monitoring can be handled at the local level, but there is a need for guidance and technical assistance. Wave forcing is another critical driver of flooding that also

deserves consideration, and future studies should focus on incorporating wave effects on flooding and erosion similar to work that has been done to predict hurricane impacts (Lynett et al., 2010; Sheng et al., 2010; Storesund et al., 2010).

5. Conclusions

Inundation of urbanized embayments by extreme high tides is challenging to predict for a number of reasons starting with the patchwork of public and private infrastructure that is relied upon for flood defense. This varies considerably in construction quality and condition and must be carefully inspected to characterize avenues for leakage, e.g., gaps between neighboring properties, cracks in structures, overtopping and seepage. Nevertheless, this study shows that accurate prediction of localized flood depths from a specific tide event is possible with a high-resolution hydraulic model if flood defenses and hydraulic pathways are comprehensively surveyed and integrated into the flood model. Furthermore, flood extent predictions are found to be very sensitive to bay water levels and barrier heights. Overprediction of bay levels or underprediction of barrier heights by only a few centimeters can cause a significant overprediction of flooding. Conversely, underprediction of bay levels and overprediction of barrier heights can cause a significant underprediction of flood extent. Therefore, to accurately map flood inundation caused by *ca.* 1–2 m amplitude tides typical of California, barrier heights should be surveyed with a vertical RMSE less than ~1 cm for use in flood mapping models. This level of accuracy can be achieved with precision surveying instrumentation such as the RTK technology used here, but LiDAR survey data with a vertical RMSE of ~15 cm is inadequate. Finally, the efficacy of temporary flood control activities such as seasonal sand berm construction and cautionary sand bagging (e.g., before a predicted high tide) is validated by the high sensitivity of flood extent to overtopping heights.

Hydraulic flood mapping is recommended over equilibrium mapping because the latter is strongly biased towards over-prediction. However, equilibrium flood mapping tools may be suitable for undefended terrain. Tidal amplification should also be considered even in small embayments to account for centimetric changes in the bay level that could trigger flooding.

Acknowledgments

This work was supported by a grant from the National Science Foundation (CMMI-0825165) and made possible by the gracious cooperation of the City of Newport Beach personnel who shared geospatial data, photographs, and invaluable site specific knowledge. The authors wish to thank the anonymous reviewers for their constructive comments on the draft manuscript.

References

Arega, F., Sanders, B.F., 2004. Dispersion model for tidal wetlands. *ASCE Journal of Hydraulic Engineering* 130 (8), 739–754.

Bates, P.D., Horritt, M.S., Smith, C.N., Mason, D., 1997. Integrating remote sensing observations of flood modeling and hydraulic modeling. *Hydrological Processes* 11 (14), 1777–1795.

Bates, P.D., Dawson, R.J., Hall, J.W., Horritt, M.S., Nicholls, R.J., Wicks, J., Hassan, M.A.A. M., 2005. Simplified two-dimensional numerical modelling of coastal flooding and example applications. *Coastal Engineering* 52 (9), 793–810.

Begnudelli, L., Sanders, B.F., 2006. Unstructured grid finite volume algorithm for shallow after transport with wetting and drying. *Journal of Hydraulic Engineering* 132 (4), 371–384.

Begnudelli, L., Sanders, B.F., Bradford, S.F., 2008. Adaptive Godunov-based model for flood simulation. *Journal of Hydraulic Engineering* 134 (6), 714–725.

Bradford, S.F., Sanders, B.F., 2002. Finite volume model for shallow-water flooding of arbitrary topography. *Journal of Hydraulic Engineering* 128 (3), 289–298.

Bradford, S.F., Sanders, B.F., 2005. Performance of high-resolution, non-level bed, shallow-water models. *Journal of Engineering Mechanics* 131 (10), 1073–1081.

Bromirski, P.D., Flick, R.E., Cayan, D.R., 2003. Storminess variability along the California coast: 1858–2000. *Journal of Climate* 16, 982–993.

Brown, J.D., Spencer, T., Moeller, I., 2007. Modeling storm surge flooding of an urban area with particular reference to modeling uncertainties: a case study of Canvey Island, United Kingdom. *Water Resources Research* 43 (W06402) doi:10.1029/2005WR004597.

Bunya, S., Dietrich, J.C., Westerlink, J.J., Ebersole, B.A., Smith, J.M., Atkinson, J.H., Jensen, R., Resio, D.T., Luettich, R.A., Dawson, C., Cardone, V.J., Cox, A.T., Powell, M.D., Westerlink, H.H., Roberts, H.J., 2010. A high-resolution coupled riverine flow, tide, wind, wind wave and storm surge model for southern Louisiana and Mississippi. Part I: model development and validation. *Monthly Weather Review* 138 (2), 345–377.

Cayan, D., Tyree, M., Dettinger, M., Hidalgo, H., Das, T., Maurer, E., Bromirski, P., Graham, N., Flick, R., 2009. Climate change scenarios and sea level rise estimates for the California 2008 Climate Change Scenarios Assessment. California Climate Change Center, Sacramento.

Cea, L., French, J.R., Vazquez-Cendon, M.E., 2006. Numerical modelling of tidal flows in complex estuaries including turbulence: An unstructured finite volume solver and experimental validation. *International Journal for Numerical Methods in Engineering* 67, 1909–1932.

Colby, J.D., Dobson, J.G., 2010. Flood modeling in the coastal plains and mountains: Analysis of terrain resolution. *Natural Hazards Review* 11 (1), 19–28.

Dawson, R.J., Dickson, M.E., Nicholls, R.J., Hall, J.W., Walkden, M.J.A., Stansby, P., Mokrech, M., Richards, J., Zhou, J., Milligan, J., Jordan, A., Pearson, S., Rees, J., Bates, P., Koukoulas, S., Watkinson, A., 2009. Integrated analysis of risks of coastal flooding and cliff erosion under scenarios of long term change. *Climatic Change* 95 (1–2), 249–288.

Defra, 2005. Making space for water: Taking forward a new government strategy for flood and coastal erosion risk management in England London Department of Environment Food and Rural Affairs. Accessed 13 July 2010 <http://library.coastweb.info/269/1/1stres.pdf>.

Ernts, J., Dewals, B.J., Detrembleur, S., Archambeau, P., Ercicum, S., Piroton, M., 2010. Micro-scale flood risk analysis based on detailed 2D hydraulic modelling and high resolution geographic data. *Natural Hazards Review* 55, 181–209.

Fewtrell, T.J., Bates, P.D., Horitt, M., Hunter, N.M., 2008. Evaluating the effect of scale in flood inundation modelling in urban environments. *Hydrological Processes* 22, 5107–5118.

Flick, R.E., 1986. A review of conditions associated with high sea levels in Southern California. *The Science of the Total Environment* 55, 251–259.

Flick, R.E., 1998. Comparison of California tides, storm surges, and mean sea level during the El Niño winters of 1982–1983 and 1997–1998. *Shore and Beach* 66 (3), 7–11.

Flick, R.E., Murray, J.F., Ewing, L.E., 2003. Trends in United States tidal datum statistics and tide range. *Journal of Waterway, Port, Coastal and Ocean Engineering* 129 (4), 155–164.

Gallegos, H.A., Schubert, J.E., Sanders, B.F., 2009. Two-dimensional, high-resolution modeling of urban dam-break flooding: A case study of Baldwin Hills, California. *Advances in Water Resources* 32, 1323–1335.

Gesch, D.B., 2009. Analysis of lidar elevation data for improved identification and delineation of lands vulnerable to sea-level rise. *Journal of Coastal Research* 25 (6), 49–58.

Graham, N.E., Diaz, H.F., 2001. Evidence for intensification of North Pacific winter cyclones since 1948. *Bulletin of the American Meteorological Society* 82, 1869–1893.

Guinot, V., 2003. Godunov-type schemes. Elsevier, Amsterdam.

Hall, J.W., Sayers, P.B., Dawson, R.J., 2005. National-scale assessment of current and future flood risk in England and Wales. *Natural Hazards* 36, 147–164.

Hall, J.W., Sayers, P.B., Walkden, M.J.A., Panzeri, I., 2006. Impacts of climate change on coastal flood risk in England and Wales: 2030–2100. *Philosophical Transactions of the Royal Society A – Mathematical, Physical and Engineering Sciences* 362 (1841), 1027–1049.

Heberger, M., Cooley, H., Herrera, P., Gleick, P.H., Moore, E., 2009. The impacts of sea-level rise on the California coast. California Climate Change Center, Sacramento.

Knowles, N., 2009. Potential inundation due to rising sea levels in the San Francisco Bay region. California Climate Change Center, Sacramento.

Lynett, P.J., Melby, J.A., Kim, D.H., 2010. An application of Boussinesq modeling to hurricane wave overtopping and inundation. *Ocean Engineering* 37 (1), 135–153.

Magellan, 2007. ProMark 3 RTK White Paper. Sidwell Company. Accessed 12 Apr. 2010 http://www.sidwellco.com/php/gps_solutions/docs/ProMark_3_RTK_White_Paper.pdf.

Mason, D.C., Horritt, M.S., Hunter, N.M., Bates, P.D., 2007. Use of fused airborne scanning laser altimetry and digital map data for digital flood modelling. *Hydrological Processes* 21 (11), 1436–1447.

Maune, D.F., Maitra, J.B., McKay, E.J., 2007. Accuracy standards and guidelines. In: Maune, D. (Ed.), *Digital elevation model technologies and applications: The DEM users manual*, 2nd Edition. American Society for Photogrammetry and Remote Sensing, Bethesda, Maryland, pp. 65–97.

National Research Council, 2009. Mapping the zone: Improving flood map accuracy. The National Academies Press, Washington, D.C.

Néelz, S., Pender, G., Villaneuva, I., Wilson, M., Wright, N.G., Bates, P.D., Mason, D., Whitlow, C., 2006. Using remotely sensed data to support flood modelling. *Water Management* 159 (1), 35–43.

Nicholls, R.J., 2002. Analysis of global impacts of sea-level rise: A case study of flooding. *Physics and Chemistry of the Earth* 27, 1455–1466.

Nicholls, R.J., Tol, R.S.J., Hall, J.W., 2007. Assessing impacts and responses to global-mean sea-level rise. In: Schlesinger, M.E., Khesghi, H.S., Smith, J., de la Chesnaye, F.C., Reilly, J.M., Wilson, T., Kolstad, C. (Eds.), *Human-induced climate change*. Cambridge University Press, pp. 119–134.

Orange County Public Works, 2009. Procedure for using OCTR. Retrieved from <http://www.ocgeomatics.com/Home/pdf/Procedure-for-UsingOCTR.pdf>.

- Pethick, J., 2001. Coastal management and sea-level rise. *Catena* 42, 307–322.
- Poulter, B., Halpin, P.N., 2008. Raster modelling of coastal flooding from sea-level rise. *International Journal of Geographical Information Science* 22 (2), 167–182.
- Purvis, M.J., Bates, P.D., Hayes, C.M., 2008. A probabilistic methodology to simulate future coastal flood risk due to sea level rise. *Coastal Engineering* 55, 1062–1073.
- Sanders, B.F., 2007. Evaluation of on-line DEMs for flood inundation modeling. *Advances in Water Resources* 30 (8), 1831–1843.
- Sanders, B.F., 2008. Integration of a shallow-water model with a local time step. *Journal of Hydraulic Research* 46 (8), 466–475.
- Sanders, B.F., Schubert, J.E., Gallegos, H.A., 2008. Integral formulation of shallow-water equations with anisotropic porosity for urban flood modeling. *Journal of Hydrology* 362, 19–38.
- Schubert, J.E., Sanders, B.F., Smith, M.J., Wright, N.G., 2008. Unstructured mesh generation and landcover-based resistance for hydrodynamic modeling of urban flooding. *Advances in Water Resources* 31 (12), 1603–1621.
- Sheng, Y.P., Alymov, V., Paramygin, V.A., 2010. Simulation of storm surge, wave, currents and inundation in the Outer Banks and Chesapeake Bay during Hurricane Isabel in 2003: The importance of waves. *Journal of Geophysical Research* 115, 1–27.
- Shewchuk, J.R., 1996. Triangle: Engineering a 2D quality mesh generator and Delaunay triangulator. Software In: Lin, M.C., Manocha, D. (Eds.), *Applied computational geometry: Towards geometric engineering*. Lecture notes in computer science, vol 1148. Springer-Verlag, pp. 203–222 <http://www-2.cs.cmu.edu/quake/triangle.htm>.
- Storesund, R., Bea, R.G., Huang, Y., 2010. Simulated wave-induced erosion of the Mississippi-Gulf outlet levees during Hurricane Katrina. *Journal of Waterway, Port, Coastal and Ocean Engineering* 136 (3), 177–189.
- Storlazzi, C.D., Griggs, G.B., 2000. Influence of El Niño-Southern Oscillation (ENSO) events on the evolution of central California's shoreline. *Geological Society of America Bulletin* 112 (2), 236–249.
- Toro, E.F., 2001. *Shock-capturing methods for free-surface shallow flows*. Wiley, Chichester, U.K.
- Tsubaki, R., Fujita, I., 2010. Unstructured grid generation using LiDAR data for urban flood inundation modeling. *Hydrological Processes* 24, 1404–1420.
- U.S. Army Corps of Engineers (USACE), 2006. Performance evaluation of the New Orleans and Southeast Louisiana hurricane protection system. Interagency Performance Evaluation Task Force, Washington, D.C.
- Villaneueva, I., Wright, N.G., 2006. Linking Riemann and storage cell methods for flood predictions. *Proceedings of the Institution of Civil Engineers: Water Management* 159 (1), 27–33.
- Webster, T.L., Forbes, D.L., Dickie, S., Shreenan, R., 2004. Flood-risk mapping for storm-surge events and sea-level rise using lidar for southeast New Brunswick. *Canadian Journal of Remote Sensing* 32 (3), 194–211.
- Wilson, M.D., Atkinson, P.M., 2005. Prediction uncertainty in floodplain elevation and its effect on flood inundation modelling. In: Atkinson, P.M., Foody, G.M., Darby, S.E., Wu, F. (Eds.), *GeoDynamics*. CRC Press, Boca Raton, Florida, pp. 185–202.
- Zetler, B.D., Flick, R.E., 1985. Predicted extreme high tides for California: 1983–2000. *Journal of Waterway, Port, Coastal and Ocean Engineering* 111 (4), 758–765.